Available online at www.sciencedirect.com
SCIENCE DIRECT®
Journal of Solid State Chemistry 178 (2005) 2036–2041
JOURNAL OF SOLID STATE CHEMISTRY
www.elsevier.com/locate/jssc

Crystal growth of $Ce_2O(CO_3)_2 \cdot H_2O$ in aqueous solutions: Film formation and samarium doping

Masashi Oikawa, Shinobu Fujihara*

Department of Applied Chemistry, Faculty of Science and Technology, Keio University, 3-14-1 Hiyoshi, Kohoku-ku, Yokohama 223-8522, Japan

Received 10 March 2005; received in revised form 8 April 2005; accepted 14 April 2005

Abstract

Crystalline cerium oxide carbonate hydrate ($Ce_2O(CO_3)_2 \cdot H_2O$) was grown in aqueous solutions at a low temperature of 80 °C under ambient pressure. When cerium nitrate was used as a starting material, large $Ce_2O(CO_3)_2 \cdot H_2O$ particles were precipitated through homogeneous nucleation and subsequent fast crystal growth. In contrast, the usage of cerium chloride was found to promote the preferential precipitation of $Ce_2O(CO_3)_2 \cdot H_2O$ on foreign substrates through heterogeneous nucleation and slow crystal growth. This phenomenon was applied to a chemical bath deposition of $Ce_2O(CO_3)_2 \cdot H_2O$ films. Immersion of glass substrates in the solution at 80 °C for typically 24 h resulted in formation of solid films with a unique morphology like a micrometer-scale brush. It was also found that samarium could be incorporated into $Ce_2O(CO_3)_2 \cdot H_2O$ during the crystal growth in the solutions, as evidenced by characteristic photoluminescence of Sm^{3+} in heating products of CeO_2. These results suggest that rare-earth oxide carbonate hydrates with a variety of compositions and morphologies can be synthesized from the aqueous solutions.

Keywords: Cerium oxide carbonate hydrate; Cerium dioxide; Chemical bath deposition; Crystal growth; Solid films; Photoluminescence

1. Introduction

Rare-earth (RE) compounds containing oxide, hydroxide and/or carbonate ions have received renewed attention because they can be applied to hydrogen production species [1] and phosphor materials including both hosts and activators [2–5]. Because such compounds are decomposed into RE oxides at elevated temperatures, their preparation has been carried out through low-temperature chemical processes. Basically, chemical routes to prepare RE compounds can be classified into three groups. One is a hydrothermal route using aqueous solutions of RE chloride or nitrate [6–10]. Urea or thiourea is often used to promote formation of desired RE compounds. Other two routes belong to a mild solution method [11] and a microwave-assisted synthesis [12]. The morphology of resultant powders and films is greatly dependent on chemical reaction conditions employed in each route. Therefore, it is important to investigate a new chemical approach for controlling and tailoring crystal growth and film formation.

Chemical bath deposition (CBD) has been known as a facile technique to produce solid films of metal chalcogenides or oxides by a single immersion of substrates in aqueous metal salt solutions through control of the solid formation kinetics [13]. The CBD process is based on three fundamental chemical reaction steps: (1) the formation or the dissociation of solvated ionic metal-ligand complexes, (2) hydrolysis of the complexes, and (3) the formation of solid phases. The progress of step 2 produces less soluble chemical species and causes a low degree of supersaturation of the solutions, which results in heterogeneous nucleation on foreign substrates in step 3. Precise control over pH and temperature is indispensable to achieve the deposition of films with desired composition, microstructure and

*Corresponding author. Fax: +81 45 566 1551.
E-mail address: shinobu@applc.keio.ac.jp (S. Fujihara).

0022-4596/$ - see front matter © 2005 Elsevier Inc. All rights reserved.
doi:10.1016/j.jssc.2005.04.017

properties. In case CBD solutions contain a certain kind of anionic species, it can be incorporated into growing crystals, possibly forming a variety of inorganic compounds.

In this work, crystal growth of cerium oxide carbonate hydrate ($Ce_2O(CO_3)_2 \cdot H_2O$) in aqueous solutions of cerium nitrate and chloride was investigated. Large $Ce_2O(CO_3)_2 \cdot H_2O$ particles were formed through homogeneous nucleation and subsequent fast crystal growth in the aqueous solution of cerium nitrate and urea. In contrast, crystalline films of $Ce_2O(CO_3)_2 \cdot H_2O$ were successfully prepared on glass substrates using the CBD method in the aqueous solution of cerium chloride and urea. The film morphology was very unique, reflecting the crystal growth of $Ce_2O(CO_3)_2 \cdot H_2O$ in the CBD process. It was also shown that samarium could be doped in $Ce_2O(CO_3)_2 \cdot H_2O$ during the crystal growth, as evidenced by its characteristic photoluminescence observed in thermally decomposed CeO_2:Sm^{3+} materials.

2. Experimental procedure

Cerium (III) nitrate hexahydrate ($Ce(NO_3)_3 \cdot 6H_2O$; 98.0% purity, Wako Pure Chemicals, Japan) and cerium (III) chloride hydrate ($CeCl_3 \cdot nH_2O$; 99.9% purity, Wako) were used as received. These chemicals and urea ($(NH_2)_2CO$; 99.0% purity, Wako) were dissolved in deionized water. Samarium (III) acetate tetrahydrate ($Sm(CH_3COO)_3 \cdot 4H_2O$; 99.9% purity, Soekawa Chemicals, Japan) was added to the resultant solution in case of preparing Sm^{3+}-doped samples (Ce:Sm = 100:1.5 in mol). Concentrations of RE ions and urea in the solution were adjusted to 0.2 and 0.5 M, respectively. In precipitating $Ce_2O(CO_3)_2 \cdot H_2O$ from the nitrate solution, bottles (20 ml in capacity) filled with the solution and sealed up were placed in a constant-temperature oven at 80 °C for 24 h. In preparing films from the chloride solution, quartz glass plates 1 mm in thickness were put into bottles (20 ml) filled with the solution and sealed up, and were kept still at 80 °C for typically 24 h in the oven. After the deposition, $Ce_2O(CO_3)_2 \cdot H_2O$ films were removed from the bottle and dried under ambient atmosphere. The precipitates containing samarium were heat-treated at 400–700 °C for 10 min to investigate their photoluminescent properties.

The crystal structure of the products was identified by X-ray diffraction (XRD) analysis with a Rigaku RAD-C diffractometer using Cu$K\alpha$ radiation. The tube voltage, the tube current, and the scan speed used were 50 kV, 100 mA, and 2°/min, respectively. The morphology was observed by field emission scanning electron microscopy (FESEM) with a Hitachi S-4700 microscope. The thermal decomposition behavior of $Ce_2O(CO_3)_2 \cdot H_2O$ was examined by thermogravimetry-differential thermal analysis (TG-DTA) with a Mac Science 2020S analyzer using a heating rate of 5 °C/min in air. Photoluminescence spectra were measured at room temperature with a Shimadzu RF-5300PC spectrofluorophotometer using a xenon lamp (150 W) as a light source. A filter was used to remove a second order peak of the excitation light in the photoluminescence measurement.

3. Results and discussion

3.1. Crystal growth of $Ce_2O(CO_3)_2 \cdot H_2O$

In the aqueous cerium nitrate solution, we observed the precipitation of $Ce_2O(CO_3)_2 \cdot H_2O$ without forming solid films after keeping at 80 °C for 24 h. Fig. 1 shows an FESEM image of the $Ce_2O(CO_3)_2 \cdot H_2O$ thus precipitated. Rod-like particles (approximately 5 μm in length and 2 μm in width) are seen as a result of fast crystal growth in the solution. The morphology observed is similar to that of $Ce_2O(CO_3)_2 \cdot H_2O$ prepared by homogeneous precipitation from aqueous solutions of cerium nitrate and urea through water bath heating at 85 °C [12].

From the cerium chloride solution, on the other hand, solid films were deposited on the glass substrates. Fig. 2 shows FESEM images of deposition products after immersion of the substrates in the solution at 80 °C for 9 and 12 h, elucidating initial stages of the film formation. At the beginning, triangular prism-shaped particles (approximately 20–30 μm in height and 5–10 μm in thickness) are precipitated on the substrate. Upon increases in the deposition time, the number of the particles increases and their size become larger. The particle morphology observed is also similar to that of $Ce_2O(CO_3)_2 \cdot H_2O$ prepared by homogeneous

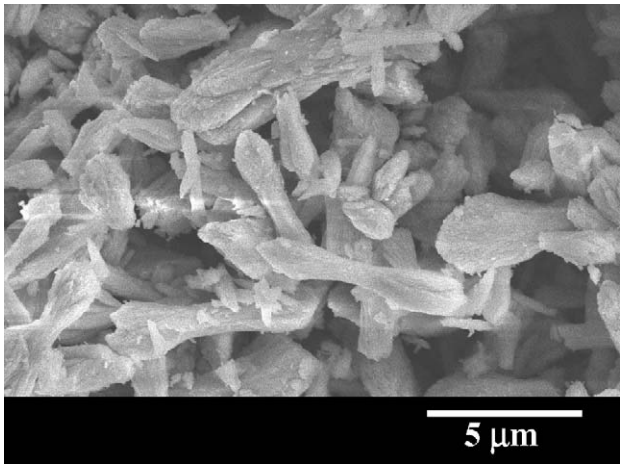

Fig. 1. An FESEM image of $Ce_2O(CO_3)_2 \cdot H_2O$ particles prepared from the cerium nitrate solution.

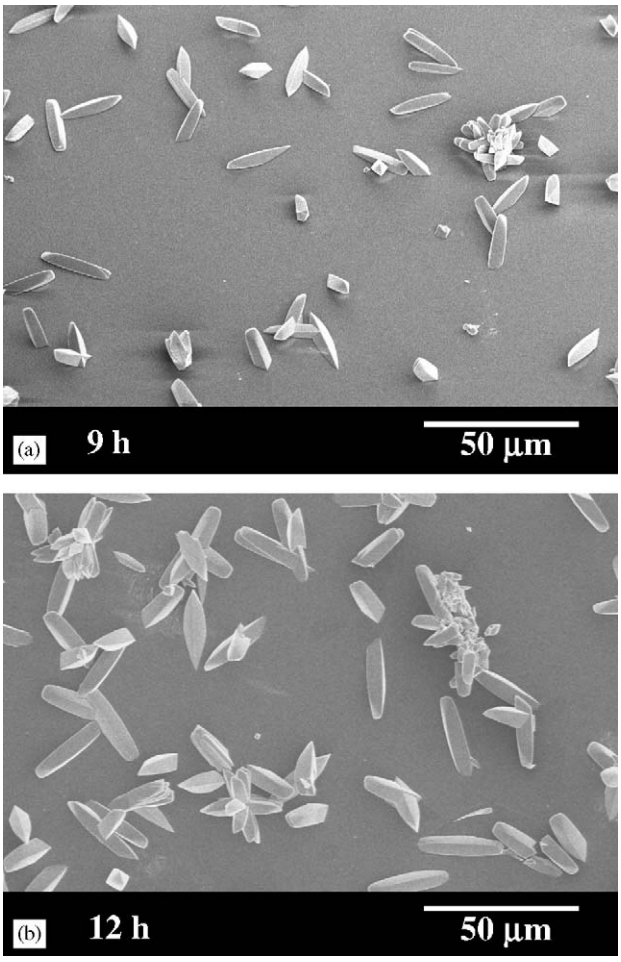

Fig. 2. FESEM images of deposition products after immersion of the substrates in the cerium chloride solution at 80 °C for 9 and 12 h.

precipitation [12]. The morphological evolution of $Ce_2O(CO_3)_2 \cdot H_2O$ can be explained on the basis of nucleation and crystal growth in solutions. Generally, solubility of solutes (Ce^{3+}, Cl^- and urea in the present case) can change as a result of chemical reactions occurring in solutions. Under the present conditions, urea can be hydrolyzed into ammonium and carbon dioxide as follows:

$$(NH_2)_2CO + H_2O \rightarrow 2NH_3 + CO_2 \quad (1)$$

The resultant ammonium further reacts with water to produce ammonium hydroxide:

$$NH_3 + H_2O \rightarrow NH_4OH \quad (2)$$

The solution then gradually becomes basic. When the solution undergoes supersaturation, solid particles are formed through nucleation and crystal growth. Although an exact reaction scheme is not clear at present, the formation of $Ce_2O(CO_3)_2 \cdot H_2O$ is supposed to be a reaction [12]:

$$2Ce^{3+} + 2OH^- + 2CO_3^{2-} \rightarrow Ce_2O(CO_3)_2 \cdot H_2O \quad (3)$$

Whether nucleation occurs homogeneously in the solutions or heterogeneously on the substrates depends on the degree of supersaturation. At lower degrees of supersaturation, occurrence of heterogeneous nucleation is much more preferential [14]. Judging from the FESEM images (Fig. 2), a degree of supersaturation of the solution is not so small at first because the large-scale particles are precipitated as a result of faster crystal growth.

After immersion of the substrates in the cerium chloride solution for 24 h, the morphology of the films deposited was dramatically changed. As shown in Fig. 3a, edge- or wedge-shaped particles (apparently 0.5–1 μm in size) are grown on the substrate, covering its surface homogeneously. High magnification FESEM images (Fig. 3b, c and d) reveal that the edges or wedges consist of nano-scaled wires, providing a brush-like morphology. Some particles seem to have grown vertically to the already existent particle surface. It is known that crystal growth in solutions proceeds with two fundamental processes: a mass transport and a surface kinetics process. In the former, the solute is transported from the bulk of the solution to the solution/crystal interface. The growth can occur primarily at kink sites at which the attachment energy is equal to the mean binding energy of the bulk crystal. The solute is finally incorporated into the crystal by the latter process. Growth can continue being driven by a steep gradient of the solute concentration generated around the growing crystal. At the late stage of the deposition, growth itself proceeds in the direction of the bulk solution from which the mass transport is in progress. As shown in Fig. 3d, the growth of each nano-scaled wire appears to be one-directional. This phenomenon is supposed to be an anion adsorption effect on the crystal growth. The chloride ion (Cl^-) can change the composition or coordination structure of the growing unit and influence the morphology through adsorption of Cl^- onto a specific crystallographic plane, as found, for example, in the anisotropic growth of rutile TiO_2 [15,16]. The fact that the film deposition behavior was different between the $CeCl_3$ and the $Ce(NO_3)_3$ solution may reflects such the effects.

The crystal structure of the film was examined by XRD, referring to Joint Committee on Powder Diffraction Standards (JCPDS, File No. 43-604). The diffraction pattern reported in the literature was also used for the phase identification [12]. Fig. 4a shows an XRD pattern of the film deposited after immersion of the substrate in the solution at 80 °C for 24 h. Ten diffraction peaks are observed in the 2θ range between 20° and 60°. These peaks correspond exactly to d values reported for $Ce_2O(CO_3)_2 \cdot H_2O$ (unindexed) in the JCPDS card ($d = 4.320$, 3.717, 2.954, 2.507, 2.347, 2.163, 2.072, 2.010, 1.823 and 1.640). Some peaks reported are absent in the pattern. However, it is very

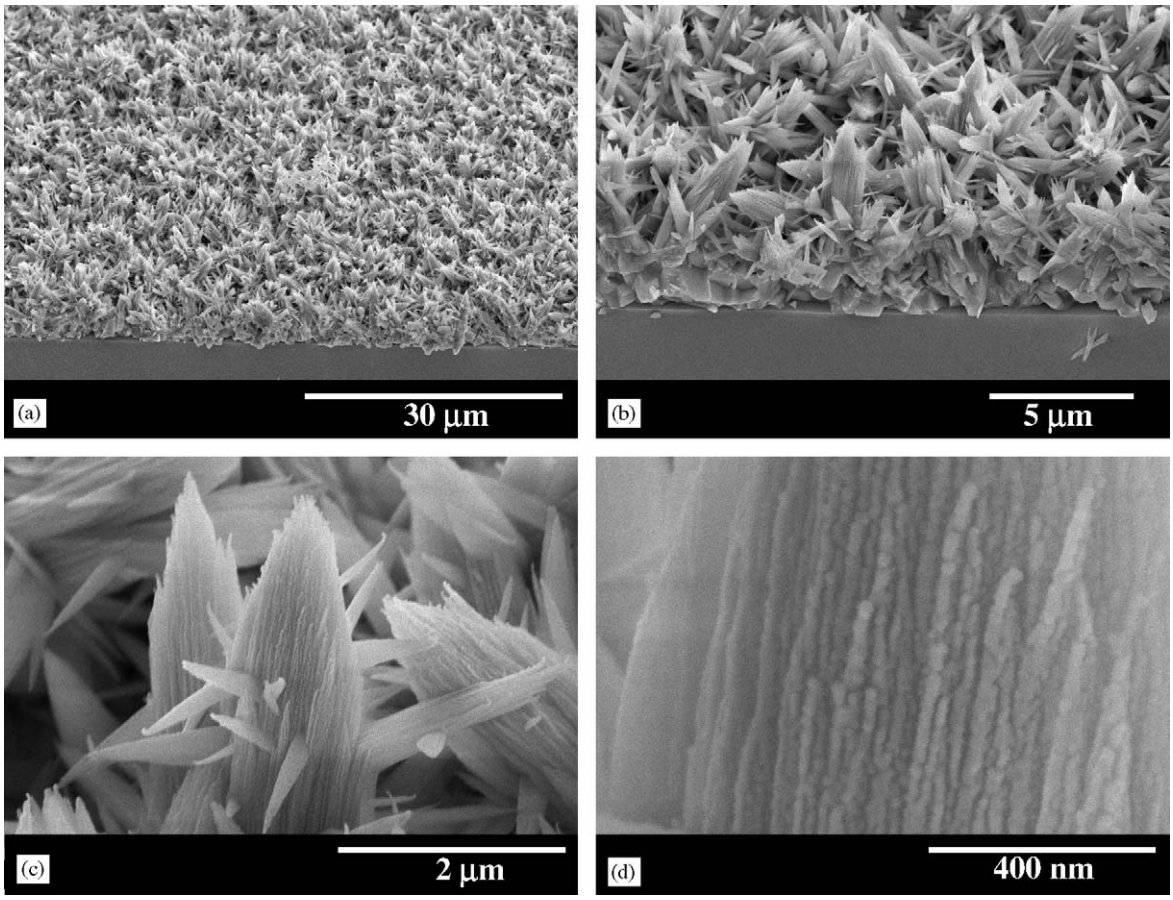

Fig. 3. Low and high magnification FESEM images of $Ce_2O(CO_3)_2 \cdot H_2O$ films deposited on the glass substrate after immersion in the cerium chloride solution at 80 °C for 24 h.

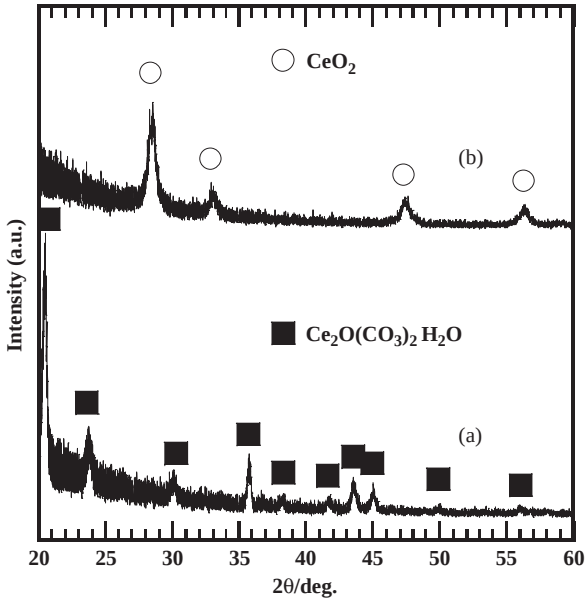

Fig. 4. XRD patterns of (a) the $Ce_2O(CO_3)_2 \cdot H_2O$ film and (b) the product obtained by heating $Ce_2O(CO_3)_2 \cdot H_2O$ at 700 °C for 10 min in air.

common that not all the peaks appear in the XRD pattern of the solid films deposited on the substrate because the $\theta-2\theta$ scan in the XRD measurement detects only the crystallographic planes parallel to the substrate surface. The microstructure of the film shown in Fig. 3 also suggests occurrence of the crystallographic orientation. The background appearing at the lower 2θ range in the pattern comes from the glass substrate because the films are not dense in the depth direction.

The thermal decomposition behavior of $Ce_2O(CO_3)_2 \cdot H_2O$ was examined by TG-DTA. For this analysis, a sample was prepared by the direct precipitation of $Ce_2O(CO_3)_2 \cdot H_2O$ in the cerium nitrate solution to collect the amount (approximately a few mg) enough for the measurement. Fig. 5 shows TG-DTA curves for the $Ce_2O(CO_3)_2 \cdot H_2O$. A small weight loss at elevated temperatures up to 200 °C is ascribed to the release of physically adsorbed water. A large weight loss is observed in the temperature range 200–250 °C. A small endothermic peak at 245 °C accompanies this weight loss. An XRD pattern of the decomposition product (heated to 700 °C) shown in Fig. 4b reveals that

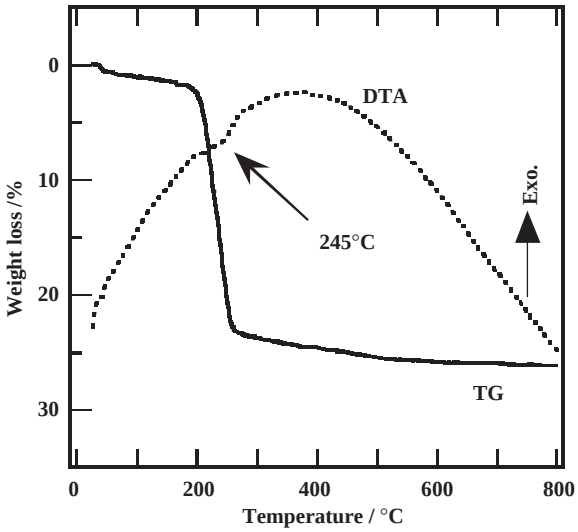

Fig. 5. TG-DTA curves for $Ce_2O(CO_3)_2 \cdot H_2O$.

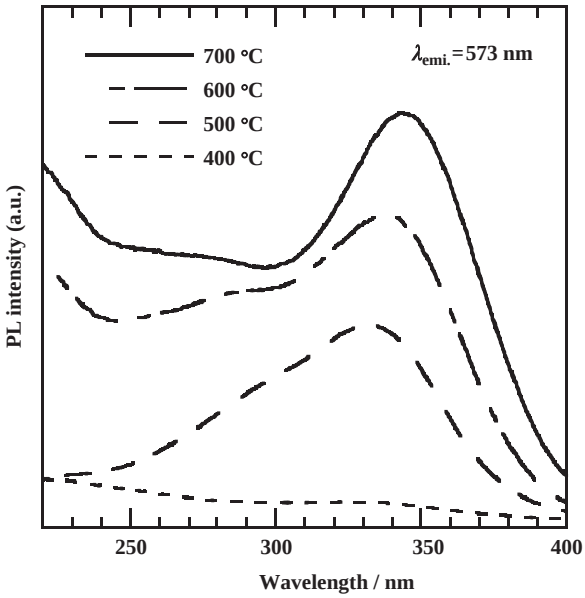

Fig. 6. Photoluminescence excitation (PLE) spectra of CeO_2:Sm^{3+} samples obtained by heating the Sm^{3+}-doped $Ce_2O(CO_3)_2 \cdot H_2O$ at 400, 500, 600 and 700 °C.

$Ce_2O(CO_3)_2 \cdot H_2O$ is transformed into CeO_2 with a cubic fluorite-type structure. A theoretical weight loss (20.7%) for the formation of CeO_2 from $Ce_2O(CO_3)_2 \cdot H_2O$ is almost the same as that observed in Fig. 5 (22%).

Possible residual nitrate or chloride species in the $Ce_2O(CO_3)_2 \cdot H_2O$ samples (both the precipitates from the nitrate solution and the films from the chloride solution) were not detected at least in X-ray photoelectron spectroscopy and Fourier transform infrared (FT-IR) spectroscopy measurements.

3.2. Samarium doping

As demonstrated in the previous works [3,4], RE compounds containing hydroxide and/or carbonate ions are good precursors for phosphor materials. Recently, we have found that Sm^{3+}-doping in CeO_2 leads to an interesting photoluminescent property [17]. Therefore, it is important to investigate whether it is possible to incorporate RE ions into $Ce_2O(CO_3)_2 \cdot H_2O$ during its crystal growth in the solutions. Sm^{3+}-doped samples were prepared from the cerium nitrate solution through the same experimental procedures as described above. According to the FESEM observation and the XRD analysis, neither the morphology nor the crystal structure of the particles was influenced by the Sm^{3+}-doping. In the photoluminescence measurement, no detectable emission was observed in the as-prepared Sm^{3+}-doped $Ce_2O(CO_3)_2 \cdot H_2O$. To examine whether the Sm^{3+} ions are present in $Ce_2O(CO_3)_2 \cdot H_2O$, we measured photoluminescence of the heat-treated CeO_2:Sm^{3+} samples. Fig. 6 shows photoluminescence excitation spectra of the CeO_2:Sm^{3+} that was obtained by heating the $Ce_2O(CO_3)_2 \cdot H_2O$ at 400, 500, 600 and 700 °C for 10 min in air. An emission wavelength used for the measurement was 573 nm, which was the strongest among emission lines observed. In the spectra, an intense, broad excitation band with a peak around 330–350 nm is observed for the CeO_2:Sm^{3+} heated at temperatures of 500, 600 and 700 °C. As we reported previously [17], the excitation of RE ions doped in CeO_2 is mainly caused by the charge transfer between the O^{2-} valence band and the Ce^{4+} conduction band and the subsequent energy transfer to RE. The O^{2-}–RE^{3+} charge transfer states lies in much higher energy levels at around 274–296 nm, which can also be observed in the photoluminescence excitation spectra in this wavelength range. The CeO_2:Sm^{3+} heated at 400 °C showed almost no emission probably because of much lower crystallinity due to the low crystallization temperature.

Fig. 7 shows the photoluminescence spectra of the CeO_2:Sm^{3+} that was heated at 400, 500, 600 and 700 °C. An excitation wavelength used was 340 nm. Spectral structures observed are characteristic of intraconfigurational f–f transitions of the RE ions. Because tetravalent cerium ions in CeO_2 have no 4f electrons, emissions are due to the presence of Sm^{3+} having five 4f electrons. This result demonstrates that the Sm^{3+}-doping in the $Ce_2O(CO_3)_2 \cdot H_2O$ precursor was successful during the crystal growth in the solutions. It can be seen that the PL intensity increases upon increases in the heat-treatment temperature, reflecting improved crystallinity with increasing temperature. Emission lines observed in Fig. 7 can be divided into two groups based on pertinent electronic transitions. One is those of magnetic-dipole $^4G_{5/2} \rightarrow {}^6H_{5/2}$ transitions (558, 561, and 573 nm) and the other is magnetic-dipole $^4G_{5/2} \rightarrow {}^6H_{7/2}$ transitions (611, 614, and 619 nm). The point-group symmetry of Ce sites in the fluorite CeO_2 structure is ideally O_h with eightfold

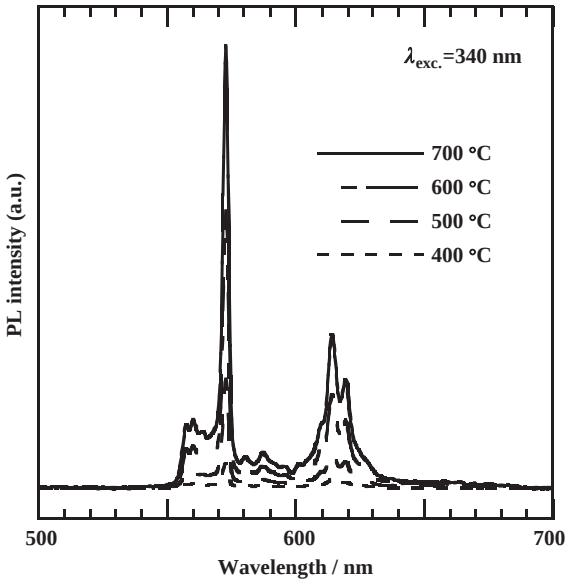

Fig. 7. Photoluminescence (PL) spectra of CeO_2:Sm^{3+} samples obtained by heating the Sm^{3+}-doped $Ce_2O(CO_3)_2 \cdot H_2O$ at 400, 500, 600 and 700 °C.

oxygen coordination, thereby providing an inversion symmetry. According to the selection rule [18], magnetic-dipole transitions that obey $\Delta J = 0$ and ± 1 (J: the total angular momentum) are allowed for Sm^{3+} in a site with inversion symmetry. Therefore, the ${}^4G_{5/2} \rightarrow {}^6H_{5/2}$ ($\Delta J = 0$) and the ${}^4G_{5/2} \rightarrow {}^6H_{7/2}$ ($\Delta J = 1$) transitions can be observed, while the ${}^4G_{5/2} \rightarrow {}^6H_{9/2}$($\Delta J = 2$) transitions, which are usually observed in other host materials, are strictly forbidden in CeO_2:Sm^{3+}. Because of the strong emission line of 573 nm, the CeO_2:Sm^{3+} exhibited bright orange color upon UV irradiation.

The occurrence of the Sm^{3+} emissions indicates that Sm^{3+} was homogeneously doped in CeO_2 without segregation as Sm_2O_3 or other Sm-related compounds. To confirm the homogeneous doping, we prepared CeO_2:Sm^{3+} thin films by a sol-gel method reported elsewhere [19] and examined their photoluminescent properties. It was concluded that more than 5% of the Sm^{3+} doping level led to the concentration quenching. This fact excludes a possibility of the formation of Sm^{3+}-related segregations in the present samples. The chemical modification of $Ce_2O(CO_3)_2 \cdot H_2O$ with other RE ions is therefore found to be possible in the chemical solution processes. Because inner 4*f* electronic configurations of RE ions contribute less to the chemical reactions, Ce^{3+} ($4f^1$) and Sm^{3+} ($4f^5$), which have the same outermost electronic configuration ($5s^2 5p^6$), can react randomly to form $Ce_2O(CO_3)_2 \cdot H_2O$. The synthesis of $Ce_2O(CO_3)_2 \cdot H_2O$ is then useful to produce Ce-based luminescent materials.

4. Conclusions

The undoped and Sm^{3+}-doped $Ce_2O(CO_3)_2 \cdot H_2O$ were prepared from the aqueous RE and urea solutions at the low temperature of 80 °C under ambient pressure. The usage of cerium nitrate led to the formation of the large particles through homogeneous nucleation and subsequent fast crystal growth. In contrast, the $Ce_2O(CO_3)_2 \cdot H_2O$ films with the unique brush-like morphology could be deposited on the glass substrates when using cerium chloride. Successful incorporation of Sm^{3+} in $Ce_2O(CO_3)_2 \cdot H_2O$ was evidenced by its characteristic photoluminescence emissions in the heat-treated CeO_2:Sm^{3+} upon irradiation of the UV light.

References

[1] E.J. Peterson, E.I. Onstott, J. Inorg. Nucl. Chem. 40 (1978) 1951.
[2] G. Blasse, L.H. Brixner, Inorg. Chim. Acta 172 (1990) 45.
[3] L.D. Vila, E.B. Stucchi, M.R. Davolos, J. Mater. Chem. 7 (1997) 2113.
[4] F.A. Sigoli, M.R. Davolos, M. Jafelicci Jr, J. Alloys Compd. 344 (2002) 308.
[5] S. Tamura, K. Koyabu, T. Masui, N. Imanaka, Chem. Lett. 33 (2004) 58.
[6] Z. Han, Y. Qian, S. Yu, K. Tang, H. Zhao, N. Guo, Inorg. Chem. 39 (2000) 4380.
[7] Z.H. Han, N. Guo, K.B. Tang, S.H. Yu, H.Q. Zhao, Y.T. Qian, J. Cryst. Growth 219 (2000) 315.
[8] C.H. Lu, H.C. Wang, Mater. Sci. Eng. B 90 (2002) 138.
[9] Z. Han, P. Xu, K.R. Ratinac, G.Q. Lu, J. Cryst. Growth 273 (2004) 248.
[10] Z. Han, Q. Yang, G.Q. Lu, J. Solid State Chem. 177 (2004) 3709.
[11] S. Chen, S.H. Yu, B. Yu, L. Ren, W. Yao, H. Cölfen, Chem. Eur. J. 10 (2004) 3050.
[12] Y. Ikuma, H. Oosawa, E. Shimada, M. Kamiya, Solid State Ionics 151 (2002) 347.
[13] T.P. Niesen, M.R. De Guire, J. Electroceram. 6 (2001) 169.
[14] W.D. Kingery, H.K. Bowen, D.R. Uhlmann, Introduction to Ceramics, second ed, Wiley, New York, 1976.
[15] H. Cheng, J. Ma, Z. Zhao, L. Qi, Chem. Mater. 7 (1995) 663.
[16] Q. Huang, L. Gao, Chem. Lett. 32 (2003) 638.
[17] S. Fujihara, M. Oikawa, J. Appl. Phys. 95 (2004) 8002.
[18] G. Blasse, B.C. Grabmaier, Luminescent Materials, Springer, Berlin, 1994.
[19] M. Oikawa, S. Fujihara, J. Eur. Ceram. Soc., in press (doi:10.1016/j.jeurceramsoc.2005.03.165).